Aerospace Science and Technology 87 (2019) 448–458

Contents lists available at ScienceDirect

Aerospace Science and Technology

www.elsevier.com/locate/aescte

Trajectory-following guidance based on a virtual target and an angle constraint

Qi Chen [a,*], Xugang Wang [a], Jing Yang [b], Zhongyuan Wang [a]

[a] School of Energy and Power Engineering, Nanjing University of Science and Technology, Nanjing 210094, People's Republic of China
[b] No. 203 Research Institute of China Ordnance Industries, Xi'an 710065, People's Republic of China

ARTICLE INFO

Article history:
Received 17 October 2018
Received in revised form 10 January 2019
Accepted 25 February 2019
Available online 28 February 2019

Keywords:
Trajectory following
LOS angle constraint
Virtual target
Nonsingular terminal sliding mode control
Guidance law with angle constraint

ABSTRACT

In this paper, a new trajectory-following guidance scheme based on the combination of the virtual target concept and a missile terminal guidance law is proposed. A line-of-sight (LOS) angle constraint is derived for the unmanned aerial vehicle (UAV) to track a virtual target moving along the reference trajectory, by which the trajectory-following problem is transformed into an angle-constrained terminal guidance problem such that well-developed terminal guidance laws can be incorporated into the design of a trajectory-following guidance scheme. The nonsingular sliding mode technique is employed to control the vehicle's LOS angle to converge to its desired value and thus to tightly track the reference trajectory. In addition, the finite-time trajectory-following position error convergence of the proposed guidance scheme is presented. The significant contribution of this paper lies in the fact that a LOS angle constraint has been presented for a virtual-target-based trajectory-following scheme, greatly enhancing the flexibility of the design of the trajectory-following guidance scheme. Numerical simulations are performed to demonstrate the performance of the proposed guidance law and its superiority over existing trajectory-following guidance laws.

© 2019 Elsevier Masson SAS. All rights reserved.

1. Introduction

Unmanned aerial vehicles (UAVs) are becoming increasingly important in both civilian and military applications, such as power line patrol, forest fire monitoring, geological surveys, and reconnaissance. In general, these missions require UAVs to converge to and then follow a reference trajectory. The reference trajectories are usually planned as straight lines, curves, or a combination of both. To achieve satisfactory autonomous flight, there is a need for a precise, robust, and effective trajectory-following guidance law. Various guidance laws have been developed for the purpose of trajectory following. Waypoint following [1,2] is a common method of trajectory following in which several waypoints are selected on the reference trajectory and the vehicle is guided to pass through all waypoints. Hota and Ghose [3] proposed an optimal trajectory-following guidance law based on Dubin's curves in two dimensions (2D), which was then further modified for three dimensions (3D) in [4]. Vector-field-based trajectory-following guidance laws [5–7] use a construction of vector fields that surround a reference trajectory and guide the vehicle toward it. These guidance laws possess good robustness but also lead to a relatively high computational load. Ratnoo et al. [8] devised an adaptive optimal trajectory-following guidance law using the linear quadratic regulator (LQR) technique. Yang et al. [9] studied the trajectory-tracking problem for a fixed-wing UAV using the error-regulation philosophy in which an adaptive nonlinear model predictive controller (NMPC) is designed to minimize both the mean and maximum errors between the reference trajectory and the UAV. Other techniques [10–16] have also been developed to follow a predetermined trajectory.

Virtual-target-based approaches lead to another class of trajectory-following guidance laws. A virtual target trajectory-following algorithm directs the vehicle to track a virtual target point moving along the reference trajectory ahead of the vehicle. Niculescu [17] developed an automatic lateral-track control law for an aerosonde UAV in which the vehicle is assumed to point directly toward the virtual target. The authors in [18–20] developed a nonlinear guidance logic (NLGL) for fixed-wing UAV trajectory following in which a virtual target point is chosen at a fixed predetermined distance from the vehicle. To overcome some of the limitations of NLGL, Gates [21] proposed a new nonlinear trajectory-following guidance law in which the distance between the vehicle and the virtual target is spring-like and supplemented by a fictitious drag force. Other improvements of NLGL can also be found in [22,23]. Liang et al. [24] proposed a virtual terminal based adaptive guidance for

* Corresponding author.
E-mail address: qichen@njust.edu.cn (Q. Chen).

https://doi.org/10.1016/j.ast.2019.02.034
1270-9638/© 2019 Elsevier Masson SAS. All rights reserved.

entry vehicles, where a virtual target was adaptively selected from a reference trajectory according to the vehicle's authority to cancel disturbances. Zhang et al. [25] proposed a trajectory-following method that employs both an outer guidance loop and an inner control loop based on a virtual target.

To chase a virtual target on the reference trajectory, missile terminal guidance laws, which are highly developed in the field of aerospace engineering, are also utilized in the design of UAV trajectory-following laws. The pure pursuit guidance law combined with the virtual target concept was used by Medagoda and Gibbens [26] for the trajectory following of fixed-wing UAVs. In this approach, the velocity of the virtual target is a function of the vehicle's velocity and the distance between the virtual target and the UAV, and the vehicle converges to the reference trajectory in a tail-chase manner. However, the pure-pursuit-based approach does not consider the target's heading information and generates a heading error in the case of curved trajectories, which causes the vehicle to converge to an offset from the reference trajectory. To overcome this drawback, Ratnoo [27] combined the trajectory shaping guidance law that was originally proposed in [28] with the concept of virtual target and formulated the trajectory shaping path-following guidance (TSPG) scheme to trace a general curved trajectory. This guidance law was proven to converge twice as fast as the pure pursuit and to result in lower trajectory-following errors. However, this approach was derived under the linearization assumption. When the heading errors are large, these linearized dynamics are no longer valid, and the guidance performance is likely to degrade. Further extension to a 3D scenario and comparisons with differential flatness (DF) approach were presented by Manjunath et al. [29] for a quadrotor UAV. The combination of the missile terminal guidance law with the virtual target concept gives rise to an attractive and prominent type of trajectory-following framework. Missile terminal guidance laws have become highly developed over the last several decades, and many excellent guidance laws have been proposed in various studies [30–32]. Therefore, if these excellent missile terminal guidance laws could be applied to track a virtual target, the trajectory-following performance could be significantly improved. Unfortunately, most missile terminal guidance laws cannot be directly incorporated into this framework because they may not possess the property of radius accordance between the vehicle and the virtual target in the way that TSPG does. Consequently, the implementation of well-developed missile terminal guidance laws in the virtual-target-based trajectory-following framework is limited. To solve this problem, we introduce the concept of a LOS angle constraint imposed on the virtual target tracking problem. This concept, which is the main contribution of this study, transforms the trajectory-following problem into a terminal guidance problem with a LOS angle constraint, resulting a novel trajectory-following guidance scheme. This approach makes it possible for well-developed missile terminal guidance laws to be incorporated into the virtual-target-based trajectory-following framework, as long as they satisfy the proposed LOS angle constraint, and greatly enriches the field of trajectory-following algorithms based on the combination of the virtual target concept and a missile terminal guidance law.

This paper is organized as follows. The formulation of the virtual-target-based trajectory-following problem is described in Sec. 2. The novel LOS angle constraint and the design of the proposed trajectory-following guidance scheme as well as the stability analysis are presented in Sec. 3. Section 4 presents the numerical simulation results and detailed comparisons with other guidance laws. Conclusions are presented in Sec. 5.

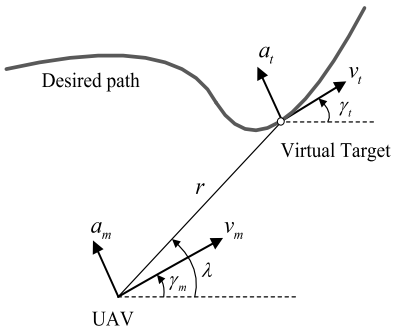

Fig. 1. Virtual-target-based guidance geometry.

2. Problem formulation

Consider the virtual-target-based trajectory-following guidance geometry shown in Fig. 1. The curve is the reference trajectory for the UAV to follow. A virtual target is assumed to move along the trajectory and to be governed by the curvature of the reference trajectory. The vehicle pursues the virtual target and reduces the distance r to converge to the reference trajectory. Here, v_m, γ_m and a_m are the vehicle velocity, vehicle heading angle and vehicle lateral acceleration, respectively. In this study, we assume that the vehicle's speed v_m is constant. v_t, γ_t and a_t are the velocity, heading angle and lateral acceleration of the virtual target, respectively. λ denotes the LOS angle. Motivated by [26], the speed of the virtual target is chosen as a function of the vehicle's speed v_m and the closing distance r as follows

$$v_t = v_m \frac{r^*}{r} \tag{1}$$

where r^* is the minimum distance between the vehicle and the virtual target that can be set as a guidance design parameter. The virtual target's speed is inversely proportional to the closing distance r. Therefore, the speed of the virtual target increases as the vehicle approaches the virtual target, which causes the vehicle to be always in pursuit of the virtual target.

With the aid of Eq. (1), the corresponding equations describing the relative motion dynamics of the vehicle and virtual target are formulated as

$$\dot{r} = v_t \cos(\lambda - \gamma_t) - v_m \cos(\lambda - \gamma_m) \tag{2}$$

$$\dot{\lambda} = \frac{1}{r}\left[-v_t \sin(\lambda - \gamma_t) + v_m \sin(\lambda - \gamma_m)\right] \tag{3}$$

$$\dot{v}_t = -\frac{r^* v_m}{r^2}\dot{r} \tag{4}$$

$$\dot{\gamma}_m = a_m / v_m \tag{5}$$

$$\dot{\gamma}_t = a_t / v_t \tag{6}$$

Differentiating Eq. (3) with respect to time yields

$$\begin{aligned}\ddot{\lambda} &= -\frac{\dot{r}}{r^2}\left[-v_t \sin(\lambda - \gamma_t) + v_m \sin(\lambda - \gamma_m)\right] \\ &\quad + \frac{1}{r}\left[-\dot{v}_t \sin(\lambda - \gamma_t) - v_t(\dot{\lambda} - \dot{\gamma}_t)\cos(\lambda - \gamma_t)\right. \\ &\quad \left. + v_m(\dot{\lambda} - \dot{\gamma}_m)\cos(\lambda - \gamma_m)\right] \\ &= -\frac{\dot{r}}{r^2}\left[-v_t \sin(\lambda - \gamma_t) + v_m \sin(\lambda - \gamma_m)\right] \\ &\quad + \frac{1}{r}\left[-\dot{v}_t \sin(\lambda - \gamma_t) + v_t \dot{\gamma}_t \cos(\lambda - \gamma_t)\right. \\ &\quad \left. - v_m \dot{\gamma}_m \cos(\lambda - \gamma_m)\right] \\ &\quad - \frac{\dot{\lambda}}{r}\left[v_t \cos(\lambda - \gamma_t) - v_m \cos(\lambda - \gamma_m)\right]\end{aligned} \tag{7}$$

Substituting Eq. (3) into Eq. (7) yields

$$\begin{aligned}\ddot{\lambda} = &-\frac{\dot{r}}{r}\dot{\lambda} + \frac{1}{r}\big[-\dot{v}_t \sin(\lambda-\gamma_t) + v_t\dot{\gamma}_t\cos(\lambda-\gamma_t)\\ &- v_m\dot{\gamma}_m\cos(\lambda-\gamma_m)\big]\\ &-\frac{\dot{\lambda}}{r}\big[v_t\cos(\lambda-\gamma_t) - v_m\cos(\lambda-\gamma_m)\big]\end{aligned} \tag{8}$$

Substituting Eq. (2) into Eq. (8), we obtain

$$\begin{aligned}\ddot{\lambda} = &-\frac{\dot{r}}{r}\dot{\lambda} + \frac{1}{r}\big[-\dot{v}_t \sin(\lambda-\gamma_t) + v_t\dot{\gamma}_t\cos(\lambda-\gamma_t)\\ &- v_m\dot{\gamma}_m\cos(\lambda-\gamma_m)\big] - \frac{\dot{\lambda}}{r}\dot{r}\end{aligned} \tag{9}$$

Substituting Eq. (4) into Eq. (9) yields

$$\begin{aligned}\ddot{\lambda} &= -\frac{2\dot{r}}{r}\dot{\lambda} + \frac{1}{r}\left[\frac{r^* v_m}{r^2}\dot{r}\sin(\lambda-\gamma_t) + v_t\dot{\gamma}_t\cos(\lambda-\gamma_t)\right.\\ &\quad\left. - v_m\dot{\gamma}_m\cos(\lambda-\gamma_m)\right]\\ &= -\frac{2\dot{r}}{r}\dot{\lambda} + \frac{\cos(\lambda-\gamma_t)}{r}v_t\dot{\gamma}_t - \frac{\cos(\lambda-\gamma_m)}{r}v_m\dot{\gamma}_m\\ &\quad + \frac{r^* v_m}{r^3}\dot{r}\sin(\lambda-\gamma_t)\end{aligned} \tag{10}$$

Substituting Eqs. (5) and (6) into Eq. (10) yields

$$\begin{aligned}\ddot{\lambda} = &-\frac{2\dot{r}}{r}\dot{\lambda} + \frac{\cos(\lambda-\gamma_t)}{r}a_t - \frac{\cos(\lambda-\gamma_m)}{r}a_m\\ &+ \frac{r^* v_m}{r^3}\dot{r}\sin(\lambda-\gamma_t)\end{aligned} \tag{11}$$

Note that, in the preceding derivation, we ignore the autopilot system of the UAV. In other words, it is assumed that the UAV can track the acceleration command instantaneously.

3. Design of the trajectory-following guidance law

3.1. LOS angle constraint for virtual target chasing

Based on the concept of virtual target pursuit, the trajectory-following problem can be transformed into a terminal guidance problem with respect to the virtual target moving on the reference trajectory. However, due to the presence of r^*, unlike in conventional missile-target engagement, here, there is no interception between the virtual target and the vehicle. To ensure precise trajectory tracking, we will show in this section that a constraint should be imposed on the "impact angle" of the vehicle during trajectory following. Because no interception occurs during the entire guidance process, the definition of the "impact angle" is different from that in [30–32]. Here, we define the "impact angle" as the LOS angle when the virtual target's speed matches the vehicle's speed, namely, when the virtual target maintains the prescribed minimum separation distance from the vehicle (i.e., $r = r^*$). The study in [27] did not use a LOS angle constraint, but TSPG still achieves accurate trajectory-following performance. This is mainly because the trajectory shaping guidance law, which is the missile terminal guidance law used in TSPG (namely, the core component of TSPG), can ensure that the vehicle's instantaneous radius of curvature is identical to that of the virtual target. Unfortunately, most terminal guidance laws do not possess this property, and trajectory-following errors occur if these guidance laws are directly used to track the virtual target. Therefore, we introduce the concept of a LOS angle constraint and extend the virtual-target-based approach to a general scenario. In this section, we present the desired LOS angle that is required for the vehicle to precisely track the reference trajectory. In most applications, the reference trajectories are commonly planned as straight lines, circular lines, or combinations of both. Therefore, we use a straight trajectory and a curve as examples to analyze the desired angle constraint.

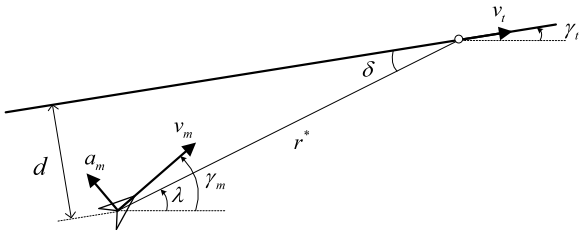

Fig. 2. Straight trajectory following when $r \to r^*$.

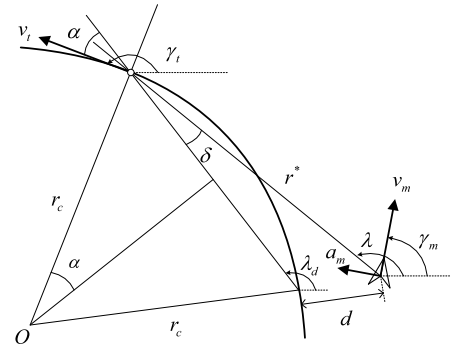

Fig. 3. Curved trajectory following when $r \to r^*$.

Theorem 1. *For straight and curved reference trajectories, if the LOS angle λ between the vehicle and the virtual target satisfies*

$$\lim_{r\to r^*}\lambda = \lambda_d \tag{12}$$

where λ_d is the desired LOS angle and is defined as $\lambda_d = \gamma_t - \arcsin(\frac{a_t}{2v_t^2}r^*)$, then it is guaranteed that the trajectory-following position error will be zero when $r \to r^*$.

Proof. For a straight trajectory, Fig. 2 presents the trajectory-following schematic diagram when $r \to r^*$. Here, d is the trajectory-following error, and δ is the angle between the LOS and the reference straight trajectory.

According to the geometrical relationship shown in Fig. 2, we obtain

$$\delta = \lambda - \gamma_t \tag{13}$$

Assuming small angles, δ can be approximated as

$$\delta \approx \frac{d}{r^*} \tag{14}$$

Combining Eq. (13) and Eq. (14) yields

$$d \approx r^*(\lambda - \gamma_t) \tag{15}$$

For the straight trajectory, we have $a_t = 0$ and Eq. (12) becomes $\lim_{r\to r^*}\lambda = \gamma_t$. Using Eq. (15), it can be deduced that $\lim_{r\to r^*} d = 0$. Therefore, the trajectory-following position error is zero when $r \to r^*$.

For a curved trajectory, Fig. 3 shows the trajectory-following schematic diagram when $r \to r^*$. Here, r_c denotes the radius of the curve, and α denotes the ideal angle between the LOS and the virtual target's speed vector in the absence of perturbations. λ_d is the desired LOS angle in the absence of perturbations.

Assuming $d \ll 2r^*$ when $r \to r^*$, we obtain

$$\alpha \approx \arcsin \frac{r^*}{2r_c} \tag{16}$$

From the geometrical relationship shown in Fig. 3, it can be obtained that

$$\delta = \lambda - (\gamma_t - \alpha) \tag{17}$$

Assuming small angles, δ can be approximated as

$$\delta \approx \frac{d}{r^*} \tag{18}$$

Using Eqs. (17) and (18), the trajectory-following error can be expressed as

$$d \approx r^*(\lambda - \gamma_t + \alpha) \tag{19}$$

Substituting Eq. (16) into Eq. (19) yields

$$d \approx r^*\left(\lambda - \gamma_t + \arcsin \frac{r^*}{2r_c}\right) \tag{20}$$

Considering $r_c = v_t^2/a_t$, Eq. (20) can be rewritten as

$$d \approx r^*\left[\lambda - \gamma_t + \arcsin\left(\frac{a_t}{2v_t^2} r^*\right)\right] \tag{21}$$

Substituting Eq. (12) into Eq. (21), we obtain

$$\lim_{r \to r^*} d = 0 \tag{22}$$

Therefore, Eq. (12) can guarantee that the trajectory-following error d tends to zero when $r \to r^*$. The proof is completed. □

Note that the reference trajectory is planned in advance; thus, the instantaneous radius of curvature of the trajectory is known. By setting v_t according to Eq. (1), a_t can be obtained from the relation $a_t = v_t^2/r_c$. Therefore, the desired LOS angle λ_d in Eq. (12) is known at any time.

Using Eqs. (15) and (20), it can be deduced that

$$d \approx r^*(\lambda - \lambda_d) \tag{23}$$

Hence, the trajectory-following position error is simply proportional to the tracking error of the LOS angle, and r^* becomes the corresponding proportional coefficient. As a result, the position error tends to zero when λ tends to λ_d as $r \to r^*$, which implies that the vehicle can track the reference trajectory if the LOS angle is controlled to follow its desired value. In addition, it can be observed from Eq. (23) that reducing r^* is helpful in reducing the trajectory-following position error. It should be pointed out that the assumptions of small angle made in this section are only used to derive the desired LOS angle, and they are not needed to be hold in the practical applications.

It can be seen that the desired LOS angle λ_d changes with time due to the change in γ_t, a_t and v_t. By differentiating λ_d, we obtain

$$\dot{\lambda}_d = \frac{a_t}{v_t} - \frac{\mathrm{d}}{\mathrm{d}t}\left\{\arcsin\left(\frac{a_t}{2v_t^2} r^*\right)\right\} \tag{24}$$

Here, for simplicity, we omit the second term in Eq. (24) and approximate $\dot{\lambda}_d$ as

$$\dot{\lambda}_d = \frac{a_t}{v_t} \tag{25}$$

Note that this simplicity is only applied to the derivative of λ_d (i.e. $\dot{\lambda}_d$), no simplicity is assumed for λ_d. That is, the curvature of the reference trajectory is still taken into account in Eq. (12). Using Eq. (4) and differentiating Eq. (25) with respect to time yields

$$\begin{aligned} \ddot{\lambda}_d &= \frac{\dot{a}_t}{v_t} - \frac{a_t}{v_t^2}\left(-\frac{r^* v_m}{r^2}\dot{r}\right) \\ &= \frac{\dot{a}_t}{v_t} + \frac{r^* v_m}{r^2 v_t^2} a_t \dot{r} \end{aligned} \tag{26}$$

With new state variables defined as

$$x_1 = \lambda - \lambda_d, \qquad x_2 = \dot{\lambda} - \dot{\lambda}_d \tag{27}$$

Eq. (11) can be rewritten as

$$\begin{cases} \dot{x}_1 = x_2 \\ \dot{x}_2 = -\dfrac{2\dot{r}}{r}\dot{\lambda} + \dfrac{\cos(\lambda - \gamma_t)}{r} a_t - \dfrac{\cos(\lambda - \gamma_m)}{r} a_m \\ \qquad + \dfrac{r^* v_m}{r^3}\dot{r}\sin(\lambda - \gamma_t) - \dfrac{\dot{a}_t}{v_t} - \dfrac{r^* v_m}{r^2 v_t^2} a_t \dot{r} \end{cases} \tag{28}$$

In conclusion, the control objective in this study is to design a control law for a_m to ensure that the LOS angle λ converges to its desired value λ_d, i.e., x_1 and x_2 converge to zero, as $r \to r^*$. Therefore, the trajectory-following problem is transformed into a terminal guidance problem with a LOS angle constraint by utilizing the concept of a virtual target and the proposed desired LOS angle constraint.

3.2. Sliding mode guidance law

To make the LOS angle converge to the desired angle, a nonsingular terminal sliding mode control (NTSMC)-based trajectory-following guidance law is developed for the guidance system described by Eq. (28). Because a_m is multiplied by the term $\cos(\lambda - \gamma_m)$, the LOS angle cannot be controlled if $\lambda - \gamma_m = \pi/2$. However, from the dynamics of λ shown in Eq. (11), $\lambda - \gamma_m = \pi/2$ is not an equilibrium point, and hence, the lateral acceleration a_m can be used to control λ.

Now, to design the vehicle's trajectory-following guidance law using the principles of NTSMC, the following NTSMC manifold is introduced [34]

$$s = x_1 + \frac{1}{\beta} x_2^{\alpha}, \quad \beta > 0, \qquad \alpha = \frac{p}{q}, \quad p > q \tag{29}$$

where p and q are assumed to be odd integers and $1 < \alpha < 2$. Using the concept of "equivalent control" proposed by Utkin [33], the control input a_m to the system described in (28) is chosen to be the sum of an equivalent controller and a discontinuous controller in the following form [33]

$$a_m = a_m^{eq} + a_m^{disc} \tag{30}$$

where a_m^{eq} is the equivalent control component and a_m^{disc} is the discontinuous control component. To find the equivalent control component, we obtain the derivative of the NTSMC manifold by differentiating Eq. (29) as follows:

$$\dot{s} = \dot{x}_1 + \frac{\alpha}{\beta} x_2^{\alpha - 1} \dot{x}_2 \tag{31}$$

Substituting Eq. (28) into Eq. (31) yields

$$\begin{aligned} \dot{s} = x_2 + \frac{\alpha}{\beta} x_2^{\alpha-1}\Bigg[&-\frac{2\dot{r}}{r}\dot{\lambda} + \frac{\cos(\lambda - \gamma_t)}{r} a_t - \frac{\cos(\lambda - \gamma_m)}{r} a_m \\ &+ \frac{r^* v_m}{r^3}\dot{r}\sin(\lambda - \gamma_t) - \frac{\dot{a}_t}{v_t} - \frac{r^* v_m}{r^2 v_t^2} a_t \dot{r}\Bigg] \end{aligned} \tag{32}$$

The equivalent control component is the solution to the equation $\dot{s} = 0$ with respect to a_m, which is given by

$$a_m^{eq} = \frac{1}{\cos(\lambda - \gamma_m)}\left[-2\dot{r}\dot{\lambda} + a_t\cos(\lambda - \gamma_t) + \frac{r^* v_m}{r^2}\dot{r}\sin(\lambda - \gamma_t) - \frac{\dot{a}_t}{v_t}r - \frac{r^* v_m}{r v_t^2}a_t\dot{r} + \frac{r\beta}{\alpha}x_2^{2-\alpha}\right] \tag{33}$$

The discontinuous control component is chosen to be

$$a_m^{disc} = \frac{1}{\cos(\lambda - \gamma_m)}\varepsilon\,\mathrm{sign}(s) \tag{34}$$

where $\varepsilon > 0$. Note that knowledge of the virtual target information, a_t and $\dot{a}_t$, is required to implement the equivalent control component in Eq. (33). Because the virtual target is imposed on the reference trajectory and the reference trajectory is planned in advance, the curvature of the reference trajectory is known a priori, and thus, a_t and $\dot{a}_t$ are always available.

To analyze the stability of the closed-loop system with the guidance law in Eqs. (30), (33) and (34), consider the Lyapunov function candidate as $V = \frac{1}{2}s^2$. Differentiating V and substituting Eq. (32) yields

$$\begin{aligned}\dot{V} &= s\dot{s} \\ &= s\left\{x_2 + \frac{\alpha}{\beta}x_2^{\alpha-1}\left[-\frac{2\dot{r}}{r}\dot{\lambda} + \frac{\cos(\lambda - \gamma_t)}{r}a_t - \frac{\cos(\lambda - \gamma_m)}{r}a_m + \frac{r^* v_m}{r^3}\dot{r}\sin(\lambda - \gamma_t) - \frac{\dot{a}_t}{v_t} - \frac{r^* v_m}{r^2 v_t^2}a_t\dot{r}\right]\right\}\end{aligned} \tag{35}$$

Substituting Eqs. (30), (33) and (34), we obtain

$$\dot{V} = s\left[-\frac{\alpha}{\beta}x_2^{\alpha-1}\frac{\varepsilon\,\mathrm{sign}(s)}{r}\right] = -\frac{\alpha}{\beta}x_2^{\alpha-1}\varepsilon/r|s| \tag{36}$$

Because $\alpha = p/q$, where p and q are positive odd integers and satisfy $1 < p/q < 2$, therefore we have $x_2^{\alpha-1} > 0$ for $x_2 \neq 0$. Moreover, β, ε, r, and $|s|$ are all positive quantities. Therefore, $\dot{V}$ is negative define for the case of $x_2 \neq 0$, and thus, the condition for Lyapunov stability is satisfied. The system states can reach the sliding mode $s = 0$ within a finite time. Substituting the control input given in (30) into the second subequation of system (28) yields

$$\dot{x}_2 = -\frac{\alpha}{\beta}x_2^{2-\alpha} - \frac{\varepsilon}{r}\,\mathrm{sign}(s) \tag{37}$$

For the case of $x_2 = 0$,

$$\dot{x}_2 = -\frac{\varepsilon}{r}\,\mathrm{sign}(s) \tag{38}$$

Because both ε and r are positive, for $s > 0$ and $s < 0$, $\dot{x}_2 = -\varepsilon/r$ and $\dot{x}_2 = \varepsilon/r$, demonstrating that $x_2 = 0$ is not an attractor if the sliding mode has not been reached. Therefore, it is concluded that the sliding mode can be reached within a finite time from any arbitrary initial point. Once the sliding mode has been reached, due to the inherent property of NTSMC [34], the states x_1 and x_2 in the sliding mode converge to zero in a finite time that can be tuned by the design parameters shown in Eq. (29); that is, the LOS angle error reaches zero within a finite time. Hence, according to Eq. (23), within a finite time, the trajectory-following position error can converge to zero with the proposed guidance law.

For the scenario in which large initial heading angle errors occur, there exist $\dot{r} > 0$. The guidance law may not be able to steer the vehicle to approach the reference trajectory. Similar phenomena for target interception are also revealed in [31]. To avoid this problem, if $\dot{r} > 0$ occurs during the guidance process, the equivalent control component a_m^{eq} is modified to

$$a_m^{eq} = \frac{1}{|\cos(\lambda - \gamma_m)|}\left[2|\dot{r}|\dot{\lambda} + a_t\cos(\lambda - \gamma_t) + \frac{r^* v_m}{r^2}|\dot{r}|\sin(\lambda - \gamma_t) - \frac{\dot{a}_t}{v_t}r + \frac{r^* v_m}{r v_t^2}a_t|\dot{r}| + \frac{r\beta}{\alpha}x_2^{2-\alpha}\right] \tag{39}$$

whereas for $\dot{r} < 0$, Eq. (33) is still used to steer the vehicle.

4. Simulation results and comparisons

In this section, numerical examples are presented to illustrate the performance of the proposed trajectory-following guidance law. Considering the physical limitations of the UAV, the command acceleration is bounded according to the saturation function

$$a_m = \begin{cases} a_{m\mathrm{Max}}\,\mathrm{sign}(a_m) & \text{if } |a_m| \geq a_{m\mathrm{Max}} \\ a_m & \text{if } |a_m| < a_{m\mathrm{Max}} \end{cases} \tag{40}$$

where $a_{m\mathrm{Max}} = 150$ m/s^2 is the maximum acceleration that the vehicle can achieve. Note that the acceleration limits of ± 150 m/s^2 might be unfeasible for common UAV applications. However, because the emphasis of this section is to demonstrate the effectiveness and the superiority of the proposed guidance law. Therefore, to make fair comparisons with other guidance laws, here, we chose the same value of the acceleration limits that used in [27]. For the guidance problem investigated in this paper, the UAV is treated as a point of mass and the autopilot system is ignored. Consequently, the normal acceleration of the UAV is assumed to instantaneously track the guidance command a_m which is the output of the sliding mode guidance law in the following simulations. The speed of the vehicle considered in this study is 100 m/s. To alleviate chattering, the discontinuous function sign(s) is replaced with the sigmoid function

$$\mathrm{sgmf}(s) = 2\left(\frac{1}{1 + \exp(-s/\tau)} - \frac{1}{2}\right), \quad \tau > 0 \tag{41}$$

where τ is the width of the boundary layer of the sigmoid function and is set to 0.05. Note that the sigmoid function makes a continuous approximation of the discontinuous sign function. As has been analyzed in [33], by using this technique, the deviation from ideal sliding mode will be of order ϵ, where ϵ is proportional to τ. Therefore, it should be made a trade-off between maintaining close to ideal performance and achieving a smooth guidance command in practical applications. The parameters of the NTSMC manifold are selected to be $p = 5$, $q = 3$, and $\beta = 0.5$. The switch gain ε of the guidance law in (30) is selected to be 150. The minimum distance between the vehicle and the virtual target r^* is chosen to be 50 m, unless stated otherwise.

4.1. Straight trajectory following

First, the case of straight-line following with the initial vehicle heading angle $\gamma_m(0) = 90°$ is presented. The simulation results, including the vehicle trajectories, the lateral accelerations, the control energy cost profiles, the occurrence of the sliding mode on the surface $S = 0$, and the convergence of states, are shown in Fig. 4. For comparison purposes, the trajectory shaping path-following guidance (TSPG) presented in [27] is also applied in the simulation. The points A and B in Fig. 4 correspond to the time instants at which the sliding mode occurs and the states of system (28) converge to zero, respectively. From Fig. 4a, it is clear that both guidance laws follow the reference trajectory with negligible errors but in different manners. TSPG drives the vehicle with a tail-chase approach (moves left first) to the virtual target and results in the initial application of a high lateral acceleration (see Fig. 4b) as well

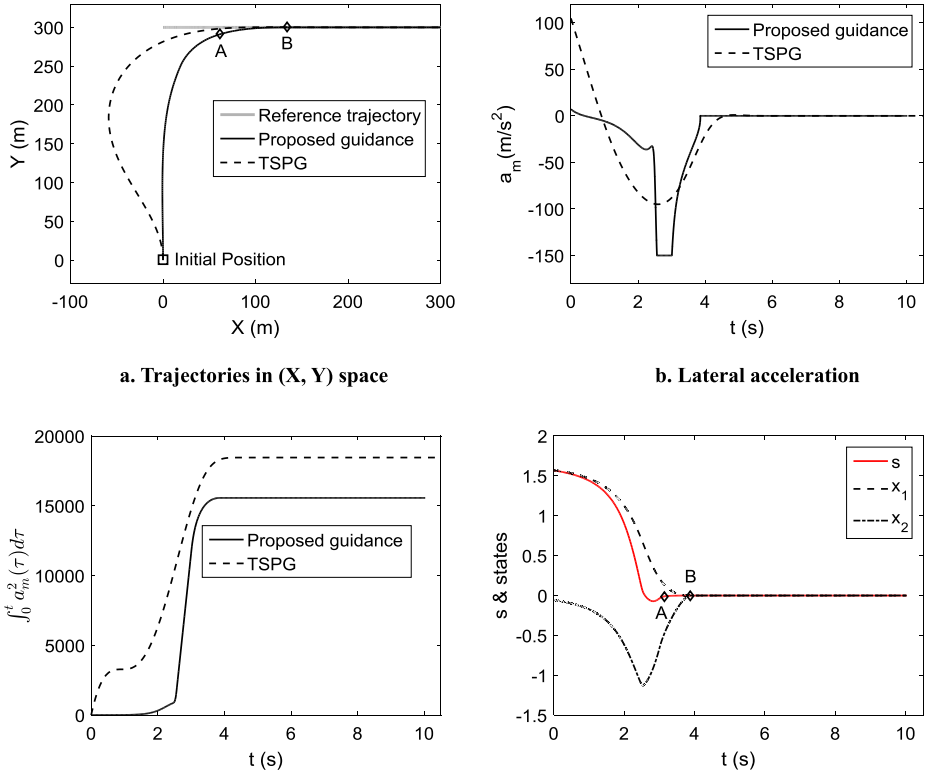

a. Trajectories in (X, Y) space **b. Lateral acceleration**

c. Control energy cost **d. Occurrence of the sliding mode and convergence of states**

Fig. 4. Straight-line following with $\gamma_m(0) = 90°$.

as a long transition distance. By contrast, the proposed guidance provides a direct way for the vehicle to move close to the reference trajectory. As a consequence, the position convergence of the proposed guidance is faster than that of TSPG. In addition, it is clearly evident from Fig. 4c that the control energy cost of the proposed guidance is less than that of TSPG. The results show the superiority of the proposed guidance over TSPG. It can be noted from Fig. 4d that the sliding mode occurs within a finite time represented by point A; the LOS angle and its rate converge to their desired value in a finite time, represented by point B. This observation is identical to the inherent finite convergence property of the NTSMC algorithm.

The same guidance laws are implemented to follow a straight line but from the initial heading angle of 180°, and the simulation results are shown in Fig. 5. Similarly, the sliding mode occurs at point A in this figure, and the desired LOS angle is tracked at point B. As seen in Fig. 5a, both guidance laws steer the vehicle to the reference trajectory even with a large initial heading error, but TSPG guides the vehicle along a longer trajectory throughout the engagement. As a consequence, TSPG achieves a lower convergence rate than the proposed guidance does. Fig. 5b presents the phase plot of the dynamics of the desired LOS angle error in which the reaching phase, represented by the segment from the start of the engagement to point A, and the sliding mode phase, represented by the segment from point A to point B, can be clearly observed.

The performance results for the guidance laws with initial heading angles of 0° and −90° are shown in Fig. 6. As seen in Fig. 6a, for the initial heading angle of 0°, the proposed guidance law provides a shorter trajectory throughout the engagement than that of TSPG and thus achieves a faster convergence rate, which is validated by Fig. 6c. Fig. 6b presents the switching surface deviations, showing that the proposed guidance can enforce the sliding mode in the presence of large initial heading angle errors; thus, the LOS angle and its rate can converge to zero in a finite time.

4.2. Curved trajectory following

The performance results for the proposed guidance as well as TSPG, pure pursuit [26], and nonlinear guidance [18,20] when tracking a circular trajectory from an initial heading angle of 0° are shown in Fig. 7. In this case, the radius of the arc is 500 m. For a fair comparison, the parameter L_1 used in nonlinear guidance is selected to be the same as r^*. It can be observed from Fig. 7a that the proposed guidance, nonlinear guidance, and TSPG can drive the vehicle to follow the reference circular trajectory, but pure pursuit has a high trajectory-following error. The lateral controls, shown in Fig. 7b, exhibit initial saturation in the case of the proposed guidance, nonlinear guidance, and TSPG, which can guide the vehicle to orient itself toward the reference trajectory as quickly as possible.

Fig. 8 presents the trajectory-following results with steady winds. In this figure, (w_x, w_y) represent the x and y components of the wind velocity. It can be observed from Fig. 8a that the proposed guidance can drive the vehicle to follow the reference trajectory quite well even in the presence of various winds. Fig. 8b provides the trajectory-following trajectories for the proposed guidance, TSPG, and nonlinear guidance with $(w_x, w_y) = (20, 20)$ m/s steady wind. Although all of the guidance laws present good trajectory following, the proposed guidance converges faster to the reference trajectory. Simulation results show that the proposed guidance is robust to the wind disturbance.

The guidance laws are implemented to follow the same circular trajectory but from an initial heading angle of 180°. The results are shown in Fig. 9. In Fig. 9a, for a large initial heading angle error, pure pursuit fails to follow the reference trajectory, and the performance of both TSPG and nonlinear guidance degrades. Moreover, TSPG drives the vehicle to initially move in the direction opposite to the reference trajectory and then guides it to slowly converge to the reference trajectory, which is less efficient in terms of distance. However, the proposed guidance achieves satisfactory trajectory-

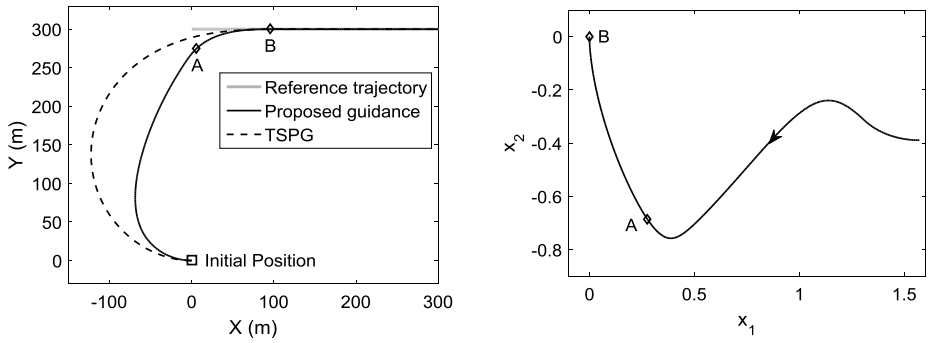

a. Trajectories in (X, Y) space **b. Trajectory in the phase plane**

Fig. 5. Straight-line following with $\gamma_m(0) = 180°$.

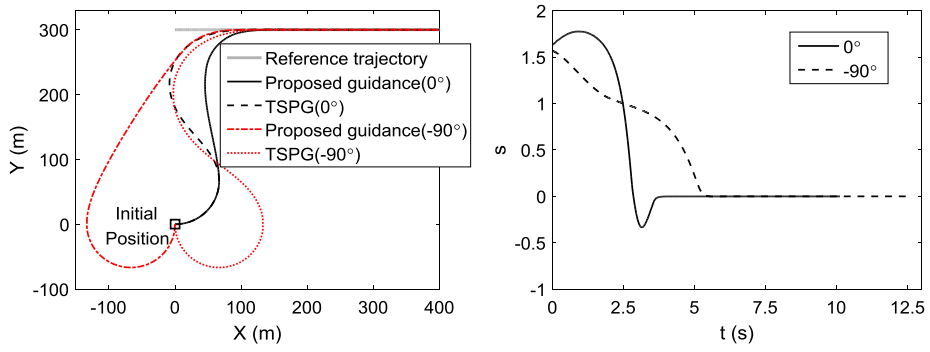

a. Trajectories in (X, Y) space **b. Occurrence of the sliding mode**

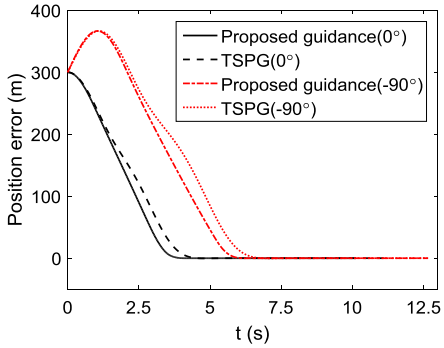

c. Position error

Fig. 6. Straight-line following with different initial heading angles.

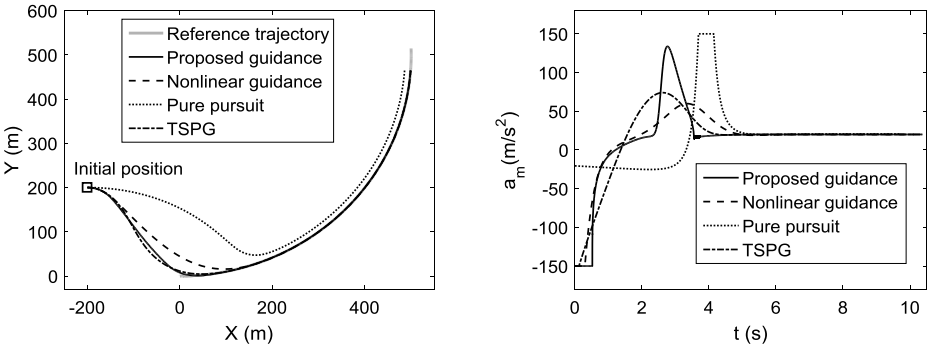

a. Trajectories in (X, Y) space **b. Lateral acceleration**

Fig. 7. Circular trajectory following with $\gamma_m(0) = 0°$.

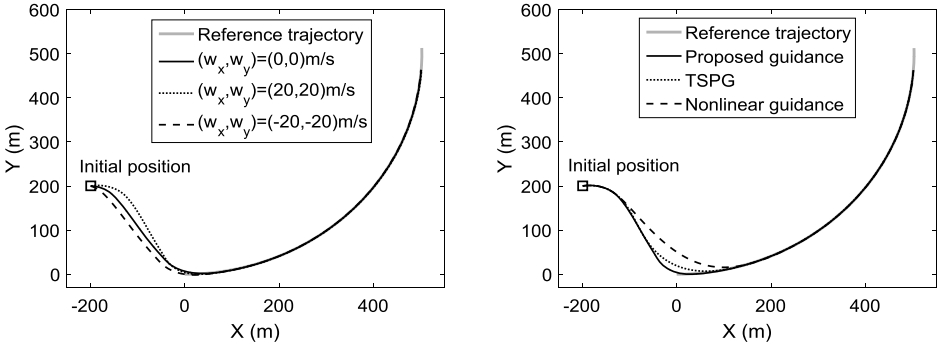

a. Trajectories of the proposed guidance **b. Comparison with (w_x,w_y)=(20,20)m/s**

Fig. 8. Circular trajectory following with winds.

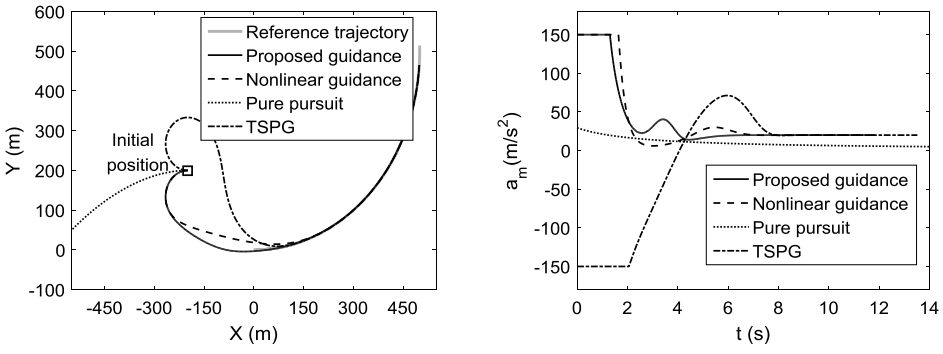

a. Trajectories in (X, Y) space **b. Lateral acceleration**

Fig. 9. Circular trajectory following with $\gamma_m(0) = 180°$.

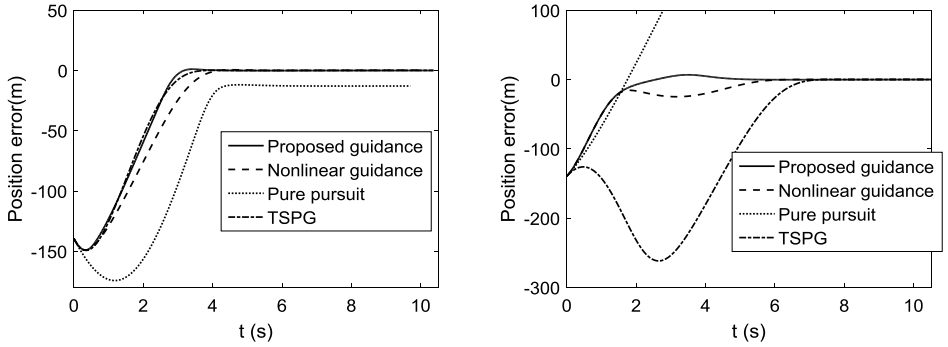

a. $\gamma_m(0)=0°$ **b. $\gamma_m(0)=180°$**

Fig. 10. Position errors with different initial heading angles.

following performance. The time histories of the position error for the preceding two cases are plotted in Fig. 10. It can be concluded that the proposed guidance not only follows the trajectory with negligible errors but also provides the fastest convergence rate. This advantage is remarkable, especially for the case of a large initial heading angle, as shown in Fig. 10b.

To demonstrate the effect of r^* selection on the performance of the guidance laws, simulations were performed with different values of r^*, ranging from 10 m to 130 m. The results are presented in Fig. 11. For this study, a composite trajectory segment consisting of a counterclockwise arc and a clockwise arc was considered.

The arc radius was set to 500 m. The guidance parameter L_1 for nonlinear guidance was chosen to be the same as r^*. As shown in Fig. 11a, for a small value of r^*, all of the guidance laws provide good trajectory following. For an increased $r^* = 70$ m, as shown in Fig. 11b, pure pursuit slowly converges and incurs considerable trajectory-following errors. The proposed guidance law, nonlinear guidance, and TSPG still follow the reference trajectory with negligible errors. However, the proposed guidance law converges more quickly to the reference trajectory. The trajectories for $r^* = 130$ m, depicted in Fig. 11c, show that the pure pursuit trajectory-following error further increases, and the nonlinear guidance performance begin to deteriorate. Both the proposed guidance law and TSPG follows the reference trajectory with negligible errors even with large values of r^*, but the proposed guidance law again provides the fastest convergence rate. These results show that the proposed guidance law is very robust with respect to the selection of r^*.

Next, an 8-shaped trajectory was considered to further evaluate the trajectory-following performance of the guidance laws. The

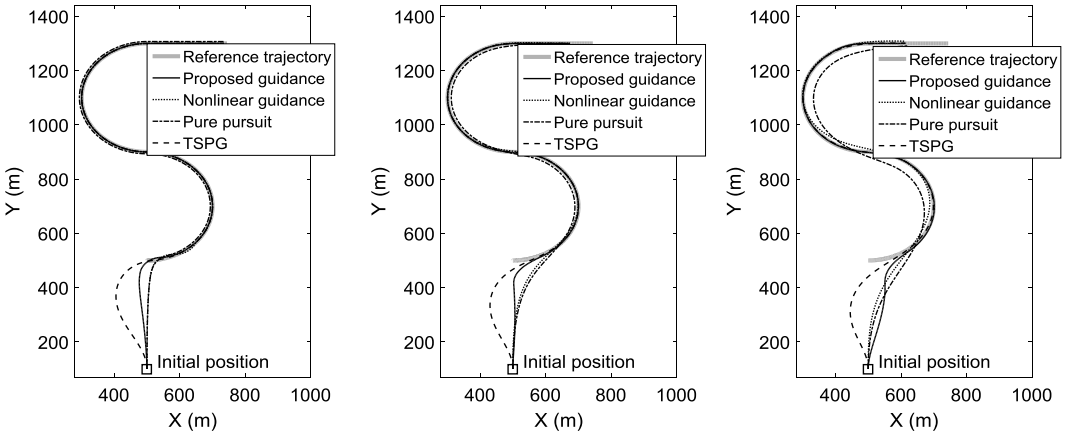

a. r^*=10 m b. r^*=70 m c. r^*=130 m

Fig. 11. Trajectories with different r^*.

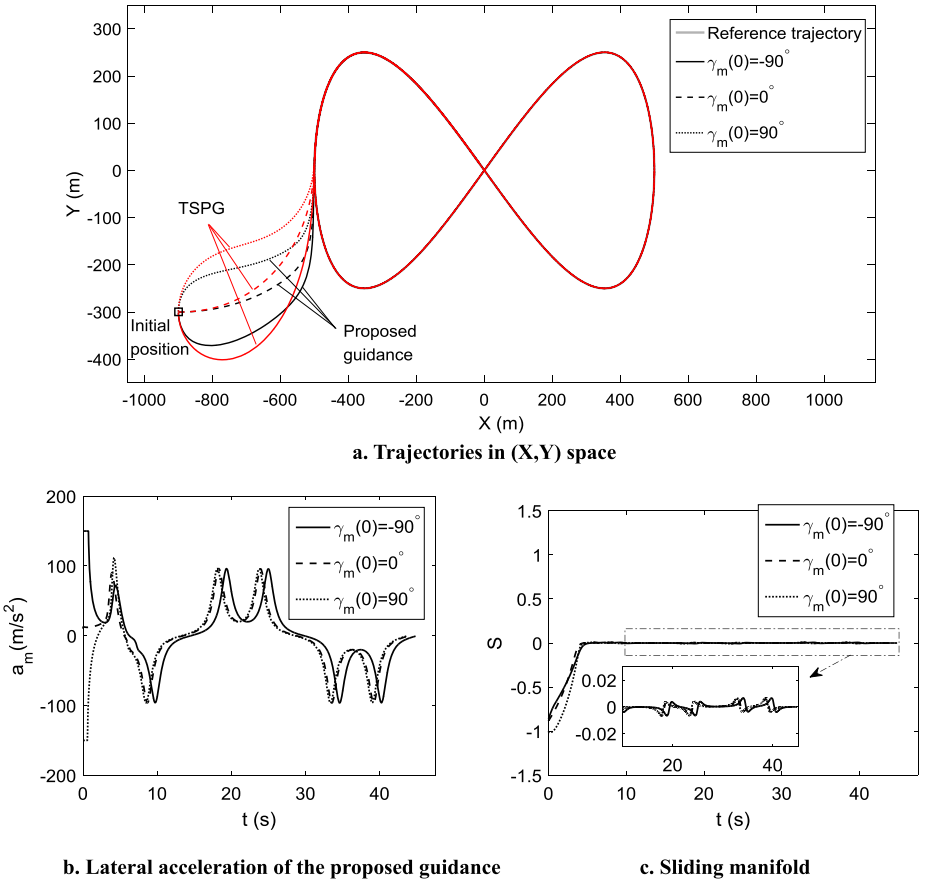

a. Trajectories in (X,Y) space

b. Lateral acceleration of the proposed guidance c. Sliding manifold

Fig. 12. 8-shaped trajectory following with different $\gamma_m(0)$.

simulation results for the proposed guidance and TSPG with different initial heading angles are shown in Fig. 12. As can be seen, both the proposed guidance and TSPG provide satisfactory trajectory following even though the reference trajectory has aggressive maneuvers. However, the proposed guidance achieves a faster convergence rate and guides the vehicle along a shorter trajectory throughout the engagement than TSPG does. It can be observed from Fig. 12c that the sliding mode occurs in a finite time. The perturbations on the sliding manifold are mainly caused by the variations of the instantaneous curvature of the reference trajectory. Simulation results imply that the proposed guidance has good adaptability for a more generalized reference trajectory.

4.3. Effectiveness of the LOS angle constraint

As mentioned above, the LOS angle constraint described by Eq. (12) was proposed for the UAV to achieve an accurate trajectory following. To further demonstrate the effectiveness of this proposed constraint, the curved trajectory following scenario is considered again and a variation of pure pursuit with the LOS angle constraint is investigated in this section.

As shown in section 4.2, pure pursuit has an obvious trajectory-following error when tracking a curved reference trajectory, while section 3.1 declares that the trajectory-following error will be zero if the proposed LOS angle of constraint of Eq. (12) is accurately

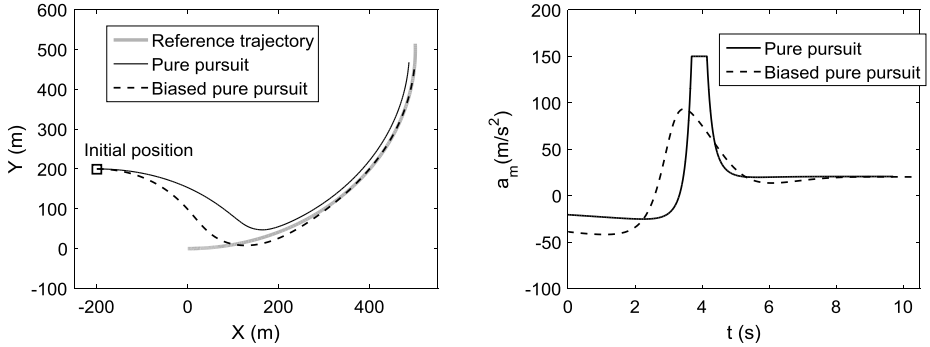

a. Trajectories in (X, Y) space **b. Lateral acceleration**

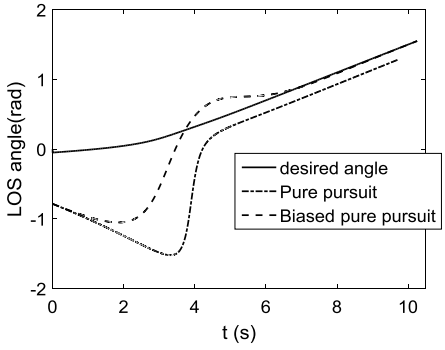

c. LOS angle tracking

Fig. 13. Circular trajectory following of different methods ($r^* = 50$ m).

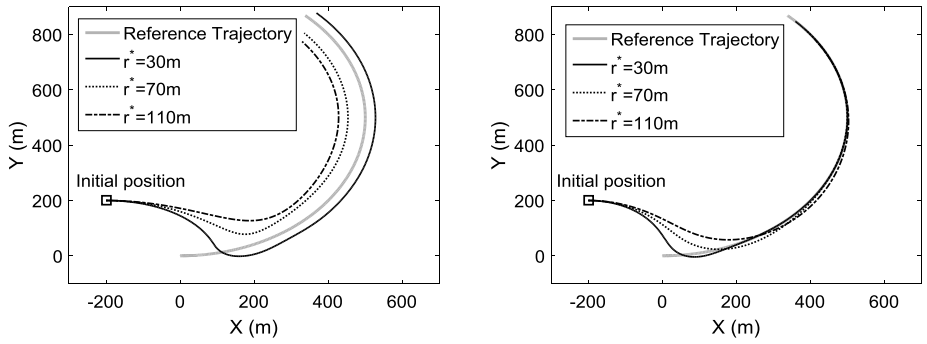

a. Pure pursuit **b. Biased pure pursuit**

Fig. 14. Comparisons of trajectories with different r^*.

tracked. Therefore, it would be interesting to assess the trajectory-following performance if pure pursuit can track the desired LOS angle as shown in Eq. (12). Unfortunately, conventional pure pursuit (i.e. $a_m = v_m\dot{\lambda}(t)$) does not possess the ability of LOS angle control. To this end, a biased pure pursuit [35] is applied and formulate as

$$\begin{cases} a_m = N_G v_m\left[\dot{\lambda}(t) - \dot{\lambda}_b(t)\right] \\ \dot{\lambda}_b(t) = \dfrac{\eta v_m[\lambda_d(t) - \lambda(t)]}{N_G r\cos[\gamma_m(t) - \lambda(t)]} \end{cases} \tag{42}$$

where N_G and η are guidance parameters, $\dot{\lambda}_b(t)$ is a biased term for the purpose of LOS angle control, $\lambda_d(t)$ is the desired LOS angle. It is clear that the biased pure pursuit adds a biased term to the conventional pure pursuit for angle control [35]. In this simulation, the guidance parameters N_G and η are selected to be 1 and 0.5, respectively.

Simulation results, including the trajectories, the lateral accelerations, and the tracking performance of the desired LOS angle, are illustrated in Figs. 13 and 14. As seen in Fig. 13a, an significant improvement of the trajectory following performance can be observed when employing the LOS angle constraint of Eq. (12). In particular, the variation of pure pursuit using the proposed LOS angle constraint drives the UAV converge to the reference trajectory quickly, whereas the conventional pure pursuit results in an obvious offset from the reference trajectory. In order to compensate the curvature of the reference trajectory, obvious adjustments of the acceleration can be observed from Fig. 13b. It is seen in Fig. 13c that biased pure pursuit successfully tracks the desired LOS angle, whereas pure pursuit has a steady-state tracking error. The simulation results shown in Figs. 13a and 13c match the analytic findings as shown in Eq. (23). Trajectories for different r^*, as shown in Fig. 14, demonstrate that the biased pure pursuit presents good trajectory following. However, the conventional pure

pursuit has considerable position errors, especially for a high value of r^*. Hence, the above comparisons indicate that the trajectory-following performance of pure pursuit is significantly improved when considering Eq. (12), demonstrating the advantage and effectiveness of the proposed LOS angle constraint.

5. Conclusions

A novel trajectory-following guidance law that combines the concept of virtual target chasing with LOS angle constrained guidance is investigated in this paper. With the help of a generalized desired LOS angle and nonsingular sliding mode control, the finite-time trajectory-following position error convergence of the proposed guidance law is theoretically proven. Moreover, the proposed guidance law addresses large initial heading angle errors with satisfactory performance. Comparisons with existing trajectory-following guidance laws in the literature and extensive simulations are presented to effectively confirm the superiority of the proposed guidance law in terms of the trajectory-following accuracy and the rate of convergence. The extension of the proposed guidance law to three-dimensional (3D) trajectory-following scenarios is an interesting possible focus of future work. Further efforts can be made in designing 3D trajectory-following guidance laws using coupled engagement dynamics and multi-dimensional switching surfaces.

Conflict of interest statement

The authors declared no potential conflicts of interest with respect to the research, authorship, and/or publication of this article.

Funding

The author(s) received no financial support for the research, authorship, and/or publication of this article.

References

[1] A. Tsourdos, B. White, M. Shanmugavel, Cooperative Path Planning of Unmanned Aerial Vehicles, vol. 32, John Wiley & Sons, 2010.
[2] Z. Liang, Q. Li, Z. Ren, Waypoint constrained guidance for entry vehicles, Aerosp. Sci. Technol. 52 (2016) 52–61.
[3] S. Hota, D. Ghose, A modified Dubins method for optimal path planning of a miniature air vehicle converging to a straight line path, in: Proceedings of the American Control Conference, IEEE, 2009, pp. 2397–2402.
[4] S. Hota, D. Ghose, Optimal geometrical path in 3D with curvature constraints, in: Proceedings of the International Conference on Intelligent Robots Systems, IEEE, 2010, pp. 113–118.
[5] D. Nelson, D. Barber, T. McLain, R. Beard, Vector field path following for miniature air vehicles, IEEE Trans. Robot. 23 (3) (2007) 519–529.
[6] D. Lawrence, E. Frew, W. Pisano, Lyapunov vector fields for autonomous UAV flight control, in: AIAA Guidance, Navigation and Control Conference and Exhibit, 2007, AIAA Paper 2007-6317.
[7] A. Pothen, A. Ratnoo, Curvature-constrained Lyapunov vector field for standoff target tracking, J. Guid. Control Dyn. 40 (10) (2017) 2725–2735.
[8] A. Ratnoo, P. Sujit, M. Kothari, Adaptive optimal path following for high wind flights, in: Proceedings of the 18th IFAC World Congress, IFAC, 2011, pp. 12985–12990.
[9] K. Yang, S. Sukkarieh, Y. Kang, Adaptive nonlinear model predictive path tracking control for a fixed-wing unmanned aerial vehicle, in: AIAA Guidance, Navigation, and Control Conference, Aug. 2009, AIAA Paper 2009-5622.
[10] J. Silva, J. Sousa, A dynamic programming approach for the motion control of autonomous vehicles, in: Proceedings of the 49th IEEE Conference on Decision Control, IEEE, 2010, pp. 6660–6665.
[11] D. Mellinger, V. Kumar, Minimum snap trajectory generation and control for quadrotors, in: 2011 IEEE International Conference on Robotics and Automation, IEEE, China, 2011, pp. 2520–2525.
[12] J. Ferrin, R. Leishman, R. Beard, T. McLain, Differential flatness based control of a rotorcraft for aggressive maneuvers, in: 2011 IEEE/RSJ International Conference on Intelligent Robots and Systems, 2011, pp. 2688–2693.
[13] A. Healey, D. Lienard, Multivariable sliding mode control for autonomous diving and steering of unmanned underwater vehicles, IEEE J. Ocean. Eng. 18 (3) (1993) 327–339.
[14] S. Ali, R. Samar, M. Shah, Nonlinear sliding manifold for high performance lateral guidance of UAV, in: Proceedings of the 36th Chinese Control Conference, China, 2017, pp. 1342–1347.
[15] S. Shehab, L. Rodrigues, Preliminary results on UAV path following using piecewise-affine control, in: Proceedings of the IEEE Conference on Control Applications, IEEE, 2005, pp. 358–363.
[16] Z. Li, J. Sun, S. Oh, Design, analysis and experimental validation of a robust nonlinear path following controller for marine surface vessels, Automatica 45 (7) (2009) 1649–1658.
[17] M. Niculescu, Lateral track control law for aerosonde UAV, in: Proceedings of the 39th AIAA Aerospace Sciences Meeting and Exhibit, 2001, AIAA Paper 2001-6575.
[18] S. Park, J. Deyst, J.P. How, A new nonlinear guidance logic for trajectory tracking, in: AIAA Guidance, Navigation, and Control Conference, Aug. 2004, AIAA Paper 2004-4900.
[19] J. Deyst, J.P. How, S. Park, Lyapunov stability of a nonlinear guidance law for UAVs, in: AIAA Atmospheric Flight Mechanics Conference and Exhibit, Aug. 2005, AIAA Paper 2005-6230.
[20] S. Park, J. Deyst, J.P. How, Performance and Lyapunov stability of a nonlinear path-following guidance method, J. Guid. Control Dyn. 30 (6) (2007) 1718–1728.
[21] D. Gates, Nonlinear path following method, J. Guid. Control Dyn. 33 (2) (2010) 321–332.
[22] M. Lizarraga, R. Curry, G. Elkaim, Flight test results for an improved line-of-sight guidance law for UAVs, in: Proceedings of the American Control Conference, IEEE, 2013, pp. 818–823.
[23] R. Curry, M. Lizarraga, B. Mairs, G. Elkaim, L_2^+, an improved line of sight guidance law for UAVs, in: Proceedings of the American Control Conference, IEEE, 2013, pp. 1–6.
[24] Z. Liang, Q. Li, Z. Ren, Virtual terminal-based adaptive predictor-corrector entry guidance, J. Aerosp. Eng. 30 (4) (2017), Article ID 04017013.
[25] J. Zhang, Q. Li, N. Cheng, B. Liang, Path-following control for fixed-wing unmanned aerial vehicles based on a virtual target, Proc. Inst. Mech. Eng., Part G, J. Aerosp. Eng. 228 (1) (2012) 66–76.
[26] E. Medagoda, P. Gibbens, Synthetic-waypoint guidance algorithm for following a desired flight trajectory, J. Guid. Control Dyn. 33 (2) (2010) 601–606.
[27] A. Ratnoo, S. Hayoun, A. Granot, T. Shima, Path following using trajectory shaping guidance, J. Guid. Control Dyn. 38 (1) (2015) 106–116.
[28] C.K. Ryoo, H. Cho, M.J. Tahk, Optimal guidance laws with terminal impact angle constraint, J. Guid. Control Dyn. 28 (4) (2005) 724–732.
[29] A. Manjunath, P. Mehrok, R. Sharma, A. Ratnoo, Application of virtual target based guidance laws to path following of a quadrotor UAV, in: Proceedings of International Conference on Unmanned Aircraft Systems, IEEE, 2016, pp. 252–260.
[30] Z. Zhang, S. Li, S. Luo, Terminal guidance laws of missile based on ISMC and NDOB with impact angle constraint, Aerosp. Sci. Technol. 31 (2013) 30–41.
[31] S. Kumar, S. Rao, D. Ghose, Nonsingular terminal sliding mode guidance with impact angle constraints, J. Guid. Control Dyn. 37 (4) (2014) 1114–1130.
[32] S. Xiong, M. Wei, M. Zhao, H. Xiong, W. Wang, B. Zhou, Hyperbolic tangent function weighted optimal intercept angle guidance law, Aerosp. Sci. Technol. 78 (2018) 604–619.
[33] V. Utkin, Sliding Modes in Control and Optimization, Springer-Verlag, Berlin, 1992.
[34] Y. Feng, X. Yu, Z. Man, Non-singular terminal sliding mode control of rigid manipulators, Automatica 38 (12) (2002) 2159–2167.
[35] B.S. Kim, J.G. Lee, H.S. Han, Biased PNC law for impact with angular constraint, Aerosp. Electron. Syst. 34 (1) (1998) 277–287.